
Flip Initial Features: Generalization of Neural Networks Under Sparse Features for Semi-supervised Node Classification

Yoonhyuk Choi¹

Jiho Choi¹

Taewook Ko¹

Chong-Kwon Kim²

¹Computer Science Dept., Seoul National University, Seoul, South Korea

²Energy AI Dept., Korea Institute of Energy Technology, Naji, South Korea

Abstract

Graph neural networks (GNNs) are commonly used in semi-supervised settings. Previous research has primarily focused on finding appropriate graph filters (e.g. aggregation methods) to perform well on both homophilic and heterophilic graphs. While these methods are effective, they can still suffer from the sparsity of node features, where the initial data contain few non-zero elements. This can lead to overfitting in certain dimensions in the first projection matrix, as training samples may not cover the entire range of graph filters (hyperplanes). To address this, we propose a novel data augmentation strategy. Specifically, by flipping both the initial features and hyperplane, we create additional space for training, which leads to more precise updates of the learnable parameters and improved robustness for unseen features during inference. To the best of our knowledge, this is the first attempt to mitigate the overfitting caused by the initial features. Extensive experiments on real-world datasets show that our proposed technique increases node classification accuracy by up to 40.2%.

Recently, many studies have focused on improving aggregation schemes for dealing with heterophilous (disassortative) edges. GNNs generally benefit from message-passing in homophilic graphs [McPherson et al., 2001], where most connected nodes are likely to share the same label. Some algorithms address this by assigning different weights to edges before aggregation [Velickovic et al., 2017, Yang et al., 2019, Bo et al., 2021, Kim and Oh, 2022] or eliminating disassortative edges [Ying et al., 2019, Luo et al., 2021]. Others use distant nodes with high similarity [Pei et al., 2020, Jin et al., 2021] and adopt node-specific propagation with trainable boundaries [Xiao et al., 2021]. We fully understand that the proper selection of aggregation schemes is essential. Nonetheless, we raise another question: *are there other aspects beyond aggregation schemes?*

Contrary to previous methods, we focus on the training of weight matrices (hyperplanes). Our investigation stems from the observation that, when initial features have few non-zero elements (e.g. bag-of-words), a shortage of training samples (in semi-supervised settings) can lead to overfitting of certain dimensions in the first layer parameters (please refer to *Appendix A* for more information). This can negatively impact the quality of predictions for test nodes with untrained dimensional features.

To better optimize the first layer projection matrix, we focused on perturbing the initial features. Our initial approach was to use a data augmentation technique such as dimensional image shifting, commonly used in computer vision [Shijie et al., 2017]. However, we found that this approach was not suitable for GNNs with bag-of-words features, as it would disrupt the semantic information. Unlike convolutional neural networks, which promote local invariance [Zhang et al., 2017], GNNs use multi-layer perceptrons (MLP), which are not translation invariant. We also considered adding noise to the inputs [Zhu et al., 2021], but this introduced additional decoding requirements, precise hyper-parameter selection, and normalization issues [Cai et al., 2021].

1 INTRODUCTION

Graph neural networks (GNNs) have achieved remarkable improvements in various fields with the influx of graphical data. By concurrently integrating node features and network structures, GNNs have demonstrated powerful capabilities in node and graph classification tasks, as demonstrated in recent studies such as [Defferrard et al., 2016, Kipf and Welling, 2016, Hamilton et al., 2017, Velickovic et al., 2017]. Message-passing, which aggregates features from neighboring nodes through recursive updates, is known as a crucial component of GNNs [Gilmer et al., 2017].

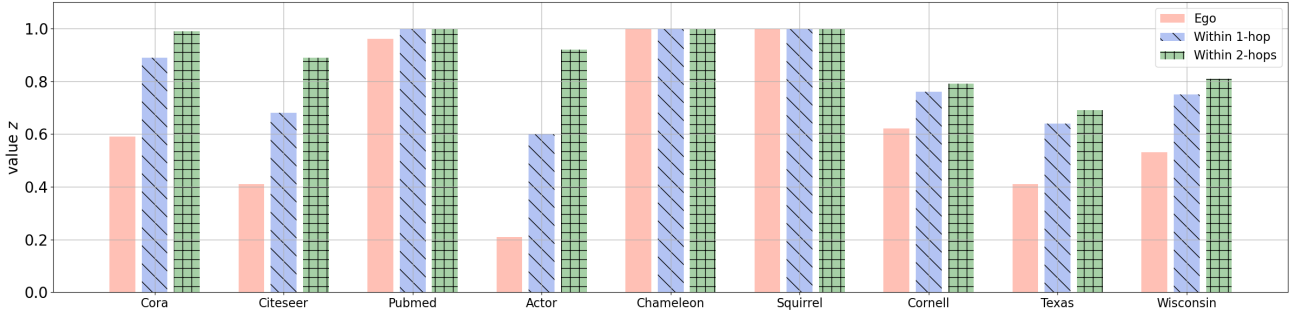


Figure 1: Initial feature distribution of each graph dataset. The definition of value z is described in Equation 1

We have devised a solution that involves flipping the initial features and parameters simultaneously. Our proposed flipping scheme is based on previous techniques such as shifting parameters [Kim et al., 2019] and rotating neural networks [Lin et al., 2020], which preserve the volume of gradients and initial features. We also focused on a dual-path network [Chen et al., 2017b] that allows for operation in both the original and flipped spaces. Our method addresses the zero gradient problem caused by input data and promotes accurate semantic learning of each dimension [Liu et al., 2022]. The flipping mechanism is orthogonal to GNNs and has been applied to three representative methods (MLP, GCN, and GAT). We compared the performance of the three flipping variants (Flip-MLP, Flip-GCN, and Flip-GAT) with state-of-the-art baselines on nine real-world datasets and observed an average gain of 16.5%, 24.2%, and 17.8% respectively. The contributions can be summarized as follows:

- We demonstrate that GNNs are highly sensitive to initial features and their performance can be significantly improved through flip-based augmentation.
- To address this issue, we propose a flipping mechanism that transposes both the initial features and hyperplane. Unlike previous methods that focus on aggregation schemes, our approach examines back-propagation and provides precise component-wise guidance for the first hyperplane.
- The proposed flipping mechanism is orthogonal to GNNs. By applying it to MLP, GCN, and GAT, we develop three flipping variants. Through extensive experiments on real-world benchmark graphs, our flipping variants outperform all existing state-of-the-art baselines significantly.

2 PRELIMINARIES

This section begins with an overview of the feature distribution in benchmark datasets. Next, we define the commonly used notations in Graph Neural Networks (GNNs), which will be utilized throughout this paper. Finally, we present the fundamental concepts of several GNN algorithms.

2.1 EMPIRICAL ANALYSIS

We conduct an empirical study to show the ratio of non-zero elements of each dataset. Firstly, let us define z as below:

$$z = \frac{\# \text{ of non-zero feature dimension in training nodes}}{\# \text{ of entire feature dimension}}, \quad (1)$$

where it contains the elements of all training nodes whose values are non-zero.

In Figure 1, we display the value of each dataset by changing the range of neighbors from ego to 2-hop neighboring nodes. As seen, z increases with the range due to the availability of more features during training. Additionally, the scale of z varies significantly for each graph, dependent on the type of input (please refer to the dataset description in § 4.1). In essence, the lower the value of z , the greater the improvement in performance obtained from flipping. To further examine this phenomenon, we provide a theoretical explanation in terms of gradient update and variance reduction in Section 3.

2.2 NOTATIONS

Let $\mathcal{G} = (\mathcal{V}, \mathcal{E})$ be an undirected graph with $|\mathcal{V}| = n$ nodes and $|\mathcal{E}| = m$ edges. The graph connectivity is represented by the adjacency matrix $A \in \{0, 1\}^{n \times n}$. Each node in the graph has properties represented by the feature matrix $X \in \mathbb{R}^{n \times F}$, where F is the number of input dimensions for the initial features. The labels of each node are represented by $Y \in \mathbb{R}^{n \times C}$, where C is the number of labels or classes.

Here, we separate the weight matrix for the first layer of the GNN into two parts, W_o and W_f , where the subscripts o and f denote the original and flipped spaces, respectively. Additionally, for gradient analysis, we take the symbol ∇ to represent the partial derivative of the loss function. The goal of this work is to solve a node classification task in a semi-supervised setting where only a subset of labeled nodes $\mathcal{V}_L \subset \mathcal{V}$ is available for training. Our focus is on how to better utilize the given features to predict the labels of unlabeled nodes $\mathcal{V}_U = \mathcal{V} - \mathcal{V}_L$.

2.3 GRAPH NEURAL NETWORK

Recently, spatial GNNs have achieved prominent performance while reducing the computational cost of Laplacian decomposition. Their basic form is given by:

$$\begin{aligned}
 H^{(l+1)} &= \sigma(\bar{H}^{(l+1)}), \quad \bar{H}^{(l+1)} = AH^{(l)}W^{(l)} \quad (l \geq 1) \\
 \hat{Y} &= \text{softmax}(\bar{H}^{(L)}).
 \end{aligned}
 \tag{2}$$

A stands for a matrix that is used for message-passing. $H^{(1)} = X$ is an initial feature of nodes and $\bar{H}^{(l)}$ is their hidden representation of l -th layer. $H^{(l)}$ can be retrieved through an activation function σ (e.g., ReLU). GNNs obtain the final prediction $\bar{H}^{(L)}$ by applying softmax on it. Here, $W^{(l)}$ is the trainable weight matrices shared across all nodes. They are updated through negative log-likelihood loss (\mathcal{L}_{nll}) between the predicted \hat{Y} and true labels Y as below:

$$\mathcal{L}_{GNN} = \mathcal{L}_{nll}(\hat{Y}, Y).
 \tag{3}$$

Generally, GNNs focus on improving aggregation schemes to determine an appropriate A [Velickovic et al., 2017, Klicpera et al., 2018, Chen et al., 2020a, Bo et al., 2021]. For instance, GCN [Kipf and Welling, 2016] uses a normalized Laplacian matrix, while GAT [Velickovic et al., 2017] creates an aggregation matrix by calculating the attention score between nodes. In the following section, we highlight the need for further investigation into the input features that previous methods may fail to generalize.

3 METHODOLOGY

3.1 MOTIVATION

We first explain the limitation of the generic GNNs. It is undeniable that appropriate aggregation schemes are essential for securing performance. However, as explained below, an aggregation scheme itself cannot solve the improper learning rooted in the sparseness of the initial features. To be more specific, we analyze the update of weight matrices $W^{(l)}$ below:

$$\nabla_{W^{(l)}} J = (AH^{(l)})^T \nabla_{\bar{H}^{(l+1)}} J, \quad l = 1, \dots, L.
 \tag{4}$$

The $J = \mathcal{L}_{GNN}$ is a full-batch loss defined in Equation 3. Intuitively, the lower value of A can obstruct the gradient flow between dissimilar nodes. Nonetheless, there arises a problem when updating the parameters of initial layer $W^{(1)}$:

$$\begin{aligned}
 \nabla_{W^{(1)}} J &= (AH^{(1)})^T \nabla_{\bar{H}^{(2)}} J \\
 &= (AX)^T \nabla_{\bar{H}^{(2)}} J.
 \end{aligned}
 \tag{5}$$

Simply, the gradient of $W^{(1)}$ is derived by differentiating J with respect to $\bar{H}^{(2)}$, and the value of AX determines the scale of a gradient. Here, the gradients become zero for certain dimensions with zero inputs ($\forall_i \in F : X_i = 0 \Rightarrow$

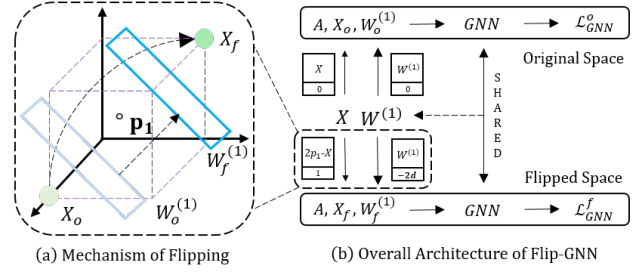


Figure 2: We describe the (a) mechanism of flipping and the (b) overall architecture of Flip-GNN. The parameter of GNN (W) is shared and updated iteratively on both spaces

($\nabla_{\bar{H}_i^{(2)}} J = 0$). Thus, the update of $W^{(1)}$ is independent of the adjacency matrix, which only relies on the sparseness of the input features. Since few training samples are available under semi-supervised settings, we focus on how to remove zero elements in X and guide $W^{(1)}$ to learn the precise meaning of each dimension.

Augmentation of input features. The inadequate gradient update described before can be more pronounced in semi-supervised learning. A simple remedy is shifting, which is commonly used in computer vision. To implement this, a small valued vector X_s can be added to the input features X as follows:

$$X = X + X_s.
 \tag{6}$$

However, shifting may not be applicable to GNNs as Multi-Layer Perceptrons (MLP) are not shift-invariant and can lead to decreased robustness [Singla et al., 2021]. Moreover, shifting changes the magnitude of an input, which is crucial for normalizing neural networks. Rotation could be a solution, but there is a possibility that some elements may take negative values. To thoroughly examine the effects of shifting, we present a simple method that combines shifting with GCN and evaluates its performance in *Appendix B*.

3.2 FLIPPED GRAPH NEURAL NETWORKS

We present a scheme that simultaneously flips both feature vectors and the hyperplane. If the original feature vector has elements in the range $[0, 1]$, then its symmetric transposition through $p_1 = (0.5, \dots, 0.5)$ will also be in this range (as seen in the hypercube in Figure 2a), with the feature vector $X_o = (1, 0, 0)$ transposing to $X_f = (0, 1, 1)$. This transposition is also applied to the hyperplane $W_o^{(1)}$. The right side of the figure shows the original and flipped spaces in the upper and lower panels, respectively. Our method utilizes a shared GNN parameter between both spaces, while the initial features X and the first hyperplane $W^{(1)}$ are varied in each iteration. For simplicity, we implement plane GCN [Kipf and Welling, 2016] as the convolution layer and the details of our approach will be discussed below.

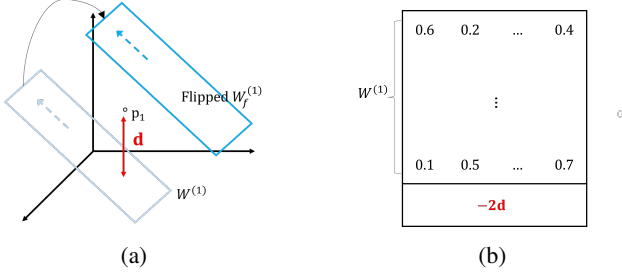


Figure 3: (a) Distance d from $W^{(1)}$ to p_1 . (b) $W_f^{(1)}$ is retrieved by padding $-2d$ to the last dimension of $W^{(1)}$, while $W_o^{(1)}$ pads 0 (please refer to Fig. 2b)

Original space. In Figure 2b, the upper panel illustrates the plane GCN. It takes X_o and $W_o^{(1)}$ as inputs, which are the zero-padded version of the initial feature matrix X and a first hyperplane $W^{(1)}$ as below:

$$X_o = \begin{pmatrix} X \\ 0 \end{pmatrix}, \quad W_o^{(1)} = \begin{pmatrix} W^{(1)} \\ 0 \end{pmatrix}. \quad (7)$$

Though the last dimension is only utilized in the flipped space, zero-padding is required to ensure dimensional consistency as $W^{(1)}$ is shared between the two spaces. Now, we can compute the loss $J_o = \mathcal{L}_{GNN}(Y, \hat{Y}_o)$ using Eq. 2 and 3, and update the parameter W . Before introducing the flipped space, we first define a symbol $p_1 = (0.5, \dots, 0.5) \in \mathcal{R}^F$, which acts as the point used for flipping. While many points could be used as p_1 (e.g., the mean of all nodes), we take the central point of F -dimensional hypercube $(1, \dots, 1) \in \mathcal{R}^F$, where most graph datasets adopt bag-of-words features.

Flipped space. The flipped feature X_f transposes X through p_1 and pads 1 as below:

$$X_f = \begin{pmatrix} X' \\ 1 \end{pmatrix}, \quad \text{where } X' = 2p_1 - X. \quad (8)$$

We should also flip the first hyperplane $W^{(1)}$ as described in Figure 3a. Firstly, we need to calculate a distance vector $d \in \mathcal{R}^{F'}$ between the original hyperplane $W^{(1)}$ and p_1 as:

$$W_f^{(1)} = \begin{pmatrix} W^{(1)} \\ -2d \end{pmatrix}, \quad \text{where } d = \sum_{j=0}^{F-1} (p_1 \otimes W^{(1)})[:, j]. \quad (9)$$

A symbol \otimes is an element-wise product. Referring to Figure 3b, $W_f^{(1)}$ is retrieved by padding $-2d$ to the last element, which makes the output of two spaces origin symmetric $X_o W_o^{(1)} = -X_f W_f^{(1)}$ (this is why we flip the hyperplane concurrently, which can preserve the pair-wise distance of hidden representations). Thus, after the first convolution layer, we should multiply negative constant to the output $\sigma(AX_f W_f^{(1)})$ before applying the next convolution as,

$$H_f^{(2)} = -\sigma(AX_f W_f^{(1)}). \quad (10)$$

Algorithm 1 The overall mechanism of Flip-GCN

Require: Adjacency matrix A , node features X , parameters θ_G , epoch K , best valid and test acc. $\gamma' = \delta' = 0$, learning rate η

Ensure: Best test accuracy δ'

- 1: **for** number of training epoch $2K$ **do**
- 2: # GCN in original space
- 3: **for** training samples **do**
- 4: Given X_o and $W_o^{(1)}$, retrieve the \mathcal{L}_{GNN}^o (Eq. 3)
- 5: Update $\theta_G^{k+1} = \theta_G^k - \eta \frac{\partial \mathcal{L}_{GNN}^o}{\partial \theta_G^k}$
- 6: **end for**
- 7: Compute the validation γ and test score δ
- 8: **if** $\gamma > \gamma'$ **then**
- 9: $\gamma' = \gamma, \delta' = \delta$
- 10: # GCN in flipped space
- 11: **for** training samples **do**
- 12: Get flipped features X_f using Eq. 8
- 13: Get flipped hyperplane $W_f^{(1)}$ using Eq. 9
- 14: Compute \mathcal{L}_{GNN}^f through Eq. 12
- 15: Update $\theta_G^{k+2} = \theta_G^{k+1} - \eta \frac{\partial \mathcal{L}_{GNN}^f}{\partial \theta_G^{k+1}}$
- 16: **end for**
- 17: Compute the validation γ and test score δ
- 18: **if** $\gamma > \gamma'$ **then**
- 19: $\gamma' = \gamma, \delta' = \delta$
- 20: **end for**

Through Eq. 10, the equality holds $H_f^{(l)} = H_o^{(l)}$ ($l \geq 2$). Thus, the following layer in a flipped space is identical to the original ones as below:

$$H_f^{(l+1)} = \sigma(\bar{H}_f^{(l+1)}), \quad \bar{H}_f^{(l+1)} = AH_f^{(l)} W^{(l)} \quad (l \geq 2). \quad (11)$$

Finally, the loss \mathcal{L}_{GNN}^f is given by:

$$\mathcal{L}_{GNN}^f = \mathcal{L}_{nll}(Y, \hat{Y}_f), \quad \text{where } \hat{Y}_f = \text{softmax}(\bar{H}_f^{(L)}). \quad (12)$$

Using Eq. 12, $W^{(1)}$ can be updated in a flipped space. We describe the overall mechanism of our method in Alg. 1.

3.3 OPTIMIZATION

We define two loss functions in Eq. 3 and 12. Before gradient analyses, please recall that the equation below holds

$$H_o^{(2)} = \sigma(AX_o W_o^{(1)}) = H_f^{(2)} = -\sigma(AX_f W_f^{(1)}), \quad (13)$$

which implies that the outputs (or gradients) of two different spaces are equivalent after two layers as below:

$$\nabla_{W_o^{(l)}} J_o = \nabla_{W_f^{(l)}} J_f \quad (l \geq 2). \quad (14)$$

Similar to J_o , the $J_f = \mathcal{L}_{GNN}^f$ is a full-batch gradient in the flipped space (Eq. 12). Though Sigmoid or Tanh

Table 1: Statistical details of nine benchmark graph datasets

Datasets	Cora	Citeseer	Pubmed	Actor	Chameleon	Squirrel	Cornell	Texas	Wisconsin
# Nodes	2,708	3,327	19,717	7,600	2,277	5,201	183	183	251
# Edges	10,558	9,104	88,648	25,944	33,824	211,872	295	309	499
# Features	1,433	3,703	500	931	2,325	2,089	1,703	1,703	1,703
# Classes	7	6	3	5	5	5	5	5	5
# Training Nodes	140	120	60	100	100	100	25	25	25
# Validation Nodes	1,568	2,207	18,657	3,750	1,088	2,550	79	79	113
# Test Nodes	1,000	1,000	1,000	3,750	1,089	2,551	79	79	113

guarantees a perfect symmetry $J_o = J_f$, we employ ReLU for better performance. Now, referring to Eq. 5, we define the gradients of the first hyperplane $W^{(1)}$ on both spaces.

In the original space, update $W_o^{(1)}$ as,

$$\nabla_{W_o^{(1)}} J_o = (AX_o)^T \nabla_{\bar{H}_o^{(2)}} J_o, \quad \bar{H}_o^{(2)} = AX_o W_o^{(1)}. \quad (15)$$

In the flipped space, update $W_f^{(1)}$ as,

$$\nabla_{W_f^{(1)}} J_f = (AX_f)^T \nabla_{\bar{H}_f^{(2)}} J_f, \quad \bar{H}_f^{(2)} = AX_f W_f^{(1)}, \quad (16)$$

where we can update the parameters of GCN including the first hyperplane $W^{(1)}$ iteratively.

Proof of convergence. We show that our optimization guarantees the convergence of $W^{(1)}$. If the activation function ensures origin symmetry, we can redefine Eq. 15 and 16 as:

$$\begin{aligned} \nabla_{W_o^{(1)}} J_o &= (AX)^T \nabla_{\bar{H}_o^{(2)}} J_o, \\ \nabla_{W_f^{(1)}} J_f &= -(A(2p_1 - X))^T \nabla_{\bar{H}_f^{(2)}} J_f. \end{aligned} \quad (17)$$

Here, the gradient of each dimension in $W^{(1)}$ is proportional to that of X and $2p_1 - X$, respectively. Also, it gets closer to a local optimum $W_*^{(1)}$ as the iteration T increases $\mathbb{E}[W_T^{(1)} - W_*^{(1)}]^2 \propto \frac{\log T}{T}$ [Li and Yuan, 2017] since the two-layer neural networks with a ReLU activation converge to a local minimum. Note that gradient ∇J and parameters $|W_o^{(l)}|, |W_f^{(l)}|$ are all bounded. These properties guarantee the convergence of Flip-GCN [Chen et al., 2017a]. Since the scale of gradients depends on the number of activated dimensions, we adjust them using α, β to stabilize our model as below:

$$\begin{aligned} W_o &= W_o - \alpha \nabla_{W_o} J_o, \\ W_f &= W_f - \beta \nabla_{W_f} J_f. \end{aligned} \quad (18)$$

We explain the design choice and computational complexity of our method in *Appendix C*.

3.4 THEORETICAL ANALYSIS

Data augmentation is closely related to empirical risk minimization, which can be explained through *bias-variance tradeoff* [Chen et al., 2020b]. Here, we prove that flipping acts as an augmentation strategy, generalizing the trainable parameters by reducing the variance of predictions. Firstly, let us assume the plane estimator as $g(X_o) = GNN(X_o)$ which is trained only with original feature X_o , and the augmented network as $\bar{g}(X) = GNN(X)$ that uses both features $X = \{X_o \cup X_f\}$. We can easily see that function g is invariant to flipping since $g(X_o, W_o) = g(X_f, W_f)$, where X_f preserves the pair-wise distance between nodes. As the bias term vanishes under the invariance, we focus on the variance of $g(X)$, which can be decomposed by the law of total variance:

$$\begin{aligned} Var(g(X)) &= Var(\mathbb{E}[g(X)]) + \mathbb{E}[Var(g(X))] \\ &= Var(\bar{g}(X)) + \mathbb{E}[Var(g(X))], \end{aligned} \quad (19)$$

where $Var(\mathbb{E}[g(X)]) = Var(\bar{g}(X))$ since they share the same marginal distribution. Here, the difference of their mean, $\mathcal{W}_1(\mathbb{E}[g(X)], \mathbb{E}[\bar{g}(X)])$, which equals to the Wasserstein distance (e.g., L_2) between two distributions is independent of the total variance. Based on this observation, we can induce the condition below:

$$Var(\bar{g}(X)) \leq Var(g(X)). \quad (20)$$

Finally, we show the losses of two networks follow:

$$\mathcal{L}(\bar{g}(X)) - \mathcal{L}(g(X)) \in -\mathbb{E}[tr(Var(g(X)))] , \quad (21)$$

which means the performance gain of an augmented model depends on the variance reduction compared to a plane method. One can induce a tighter bound of Eq. 19 and 21 using *Loewner order* [Chen et al., 2020b] but we omit them here for the brevity of explanation.

4 EXPERIMENTS

This section describes the experiments for the performance analysis. We focused our efforts to find answers to the following research questions:

Table 2: (RQ1) Node classification accuracy (%) on nine benchmark datasets. Bold with an asterisk (*) symbol indicates the best performance, and methods with † are built upon GCN. We show α, β that achieves the best accuracy (Eq. 18)

Datasets	Cora	Citeseer	Pubmed	Actor	Chameleon	Squirrel	Cornell	Texas	Wisconsin
z (Eq. 1)	0.59	0.41	0.96	0.21	1.0	1.0	0.62	0.41	0.53
Homophily (Eq. 22)	0.81	0.74	0.8	0.22	0.23	0.22	0.11	0.06	0.16
MLP	53.2 ± 0.5%	53.7 ± 1.7%	69.7 ± 0.4%	27.9 ± 1.1%	41.2 ± 1.8%	26.5 ± 0.6%	60.1 ± 1.2%	65.8 ± 5.0%	73.5 ± 5.4%
GCN†	79.1 ± 0.7%	67.5 ± 0.3%	77.8 ± 0.2%	20.4 ± 0.6%	49.4 ± 0.7%	31.8 ± 0.9%	39.4 ± 4.3%	47.6 ± 0.7%	40.5 ± 1.9%
DropEdge†	79.0 ± 0.5%	67.4 ± 0.2%	77.0 ± 0.3%	20.2 ± 0.4%	48.9 ± 1.1%	30.9 ± 0.8%	46.7 ± 3.5%	47.5 ± 2.6%	43.3 ± 4.6%
Ortho-GCN†	80.6 ± 0.4%	69.5 ± 0.3%	76.9 ± 0.3%	21.4 ± 1.6%	46.7 ± 0.5%	31.3 ± 0.6%	45.4 ± 4.7%	53.1 ± 3.9%	46.6 ± 5.8%
GIN	77.3 ± 0.8%	66.1 ± 0.6%	77.1 ± 0.7%	24.6 ± 0.8%	49.1 ± 0.7%	28.4 ± 2.2%	42.9 ± 4.6%	53.5 ± 3.0%	38.7 ± 0.5%
GAT	80.1 ± 0.6%	68.0 ± 0.7%	78.0 ± 0.4%	22.5 ± 0.3%	46.9 ± 0.8%	30.8 ± 0.9%	42.1 ± 3.1%	49.2 ± 4.4%	45.8 ± 5.3%
GATv2	79.5 ± 0.5%	67.4 ± 0.6%	76.2 ± 0.5%	22.1 ± 2.0%	48.3 ± 0.4%	28.9 ± 1.2%	38.0 ± 3.8%	52.5 ± 1.7%	41.7 ± 5.1%
APPNP	81.2 ± 0.4%	68.9 ± 0.3%	79.0 ± 0.4%	21.5 ± 0.2%	45.0 ± 0.5%	30.3 ± 0.6%	49.8 ± 3.6%	56.1 ± 0.2%	45.7 ± 1.7%
GCNII	80.8 ± 0.7%	69.0 ± 1.4%	78.8 ± 0.4%	26.1 ± 1.2%	45.1 ± 0.5%	28.1 ± 0.7%	62.5 ± 0.5%	69.3 ± 2.1%	63.2 ± 3.0%
H ₂ GCN	79.5 ± 0.6%	67.4 ± 0.5%	78.7 ± 0.3%	25.8 ± 1.2%	47.3 ± 0.9%	31.1 ± 0.5%	59.8 ± 3.7%	66.3 ± 4.6%	61.5 ± 4.4%
P-reg†	80.0 ± 0.8%	69.2 ± 0.7%	77.4 ± 0.4%	20.9 ± 0.5%	49.1 ± 0.1%	33.6* ± 0.4%	44.9 ± 3.1%	58.5 ± 4.2%	53.7 ± 2.6%
FAGCN	81.0 ± 0.3%	68.3 ± 0.6%	78.9 ± 0.4%	26.7 ± 0.8%	46.8 ± 0.6%	29.9 ± 0.5%	46.5 ± 1.7%	53.8 ± 1.2%	51.0 ± 4.1%
Flip-MLP	61.4 ± 0.7%	60.3 ± 0.5%	74.1 ± 0.5%	35.9* ± 0.5%	43.5 ± 1.2%	28.5 ± 0.8%	70.5* ± 4.1%	79.2* ± 3.6%	80.5* ± 5.1%
vs MLP (+ %)	+ 15.4 %	+ 12.1 %	+ 6.3 %	+ 28.7 %	+ 2.3 %	+ 2.1 %	+ 17.3 %	+ 20.4 %	+ 9.5 %
α, β	1, 0.1	1, 1	1, 0.01	0.1, 0.1	1, 1	1, 1	0.1, 0.1	0.1, 0.01	1, 1
Flip-GCN†	82.7 ± 0.5%	72.4 ± 0.4%	79.2* ± 0.2%	28.6 ± 0.3%	50.4* ± 0.5%	32.4 ± 0.3%	49.4 ± 0.6%	62.2 ± 1.8%	52.3 ± 2.4%
vs GCN (+ %)	+ 4.6 %	+ 7.3 %	+ 1.8 %	+ 40.2 %	+ 2.0 %	+ 1.9 %	+ 20.4 %	+ 30.7 %	+ 29.1 %
α, β	0.1, 0.01	0.01, 0.001	1, 0.01	1e ⁻⁴ , 1e ⁻⁴	1, 1e ⁻⁴	1, 0.01	1, 1e ⁻⁴	1, 1e ⁻⁴	0.01, 0.001
Flip-GAT	83.1* ± 0.6%	72.8* ± 0.4%	78.5 ± 0.2%	30.3 ± 0.8%	48.3 ± 0.3%	31.9 ± 0.5%	51.9 ± 1.4%	61.0 ± 1.1%	54.5 ± 2.1%
vs GAT (+ %)	+ 3.7 %	+ 7.1 %	+ 0.6 %	+ 34.7 %	+ 3.0%	+ 3.6 %	+ 20.2 %	+ 22.0 %	+ 19.0 %
α, β	1, 0.1	0.01, 0.001	1, 0.001	0.1, 0.1	1, 0.1	1, 1	0.1, 1e ⁻⁴	0.1, 1e ⁻⁴	0.1, 0.001

- **RQ1:** Does flipping effectively address the issue of multiple zero values in the initial features?
- **RQ2:** Does flipping ensure convergence?
- **RQ3:** How significant is the difference between the gradients from the original and flipped spaces?
- **RQ4:** How does the performance of flipping change as the number of training samples increases?

4.1 DATASETS AND BASELINES

Details of datasets. Our experiments are conducted on nine datasets whose statistical details are described in Table 1. We also measure the assortativity of each dataset as below:

$$h = \frac{\sum_{(i,j) \in \mathcal{E}} \mathbb{1}(Y_i = Y_j)}{|\mathcal{E}|}. \quad (22)$$

- **Cora, Citeseer, Pubmed** [Kipf and Welling, 2016] are citation networks. The node features in Cora and Citeseer are binary bag-of-words while Pubmed consists of TF-IDF values.
- **Actor** [Tang et al., 2009] is an actor co-occurrence graph. The node feature encodes the keywords in the actor’s Wikipedia web pages with binary values.
- **Chameleon, Squirrel** [Rozemberczki et al., 2019] are taken from Wikipedia web pages and have non-zero positive or negative values. The maximum element in each dataset is 46.4 and 70.4, while the minimum values are -0.57 and -0.99, which might not be suitable for our method.

- **Cornell, Texas, Wisconsin** contain web pages from computer science departments of multiple universities. The node features are binary bag-of-words, similar to the citation networks.

Baselines. For evaluation, we employ several traditional methods including MLP [Popescu et al., 2009], GCN [Kipf and Welling, 2016], DropEdge [Rong et al., 2019], and GIN [Xu et al., 2018]. Further, we take GAT [Velickovic et al., 2017], GATv2 [Brody et al., 2021], APPNP [Klicpera et al., 2018], GCNII [Chen et al., 2020a], H₂GCN [Zhu et al., 2020], and FAGCN [Bo et al., 2021] for heterophilous graphs. Finally, some regularization-based algorithms like P-reg [Yang et al., 2021] and Ortho-GCN [Guo et al., 2022] are used here.

We describe more details of baselines and our implementation in *Appendix D*.

4.2 RESULTS AND DISCUSSION (RQ1)

In Table 2, we observe that all flipping variants (Flip-MLP, Flip-GCN, and Flip-GAT) perform significantly better than their base models. The implementation details of Flip-MLP and Flip-GAT are discussed in *Appendix E*. We now analyze these results from two perspectives.

Performance gain of flipping is sensitive to the Z-value (Eq. 1) of each dataset. Since flipping is designed to reduce overfitting caused by the sparsity in initial features, we can easily presume that z -value, the non-zero element ratio, is the key factor that determines the performance gains of

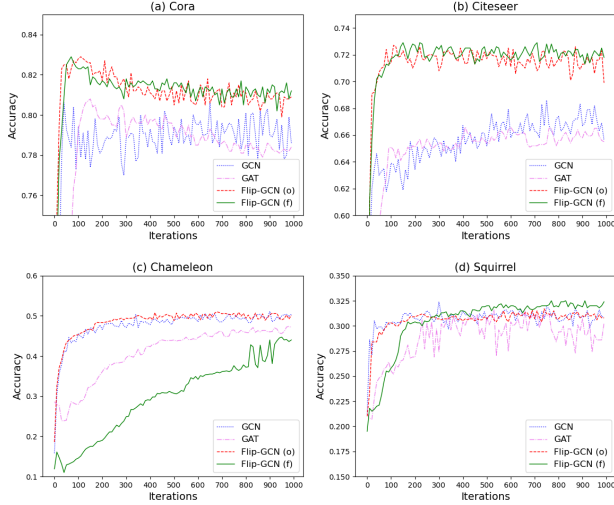


Figure 4: (RQ2) Performance of GCN, GAT, and Flip-GCN as a function of the number of iterations. The performance of Flip-GCN is measured in the original (*o*) and flipped (*f*) space, respectively

flipping. Indeed, flipping attains larger performance gains on low z -valued datasets than on higher ones. For three datasets with higher z (Pubmed, Chameleon, and Squirrel), the advancement of flipping over their vanilla models (e.g., Flip-MLP vs MLP) is relatively small. However, all three flipping methods perform better than the original methods achieving average gains of 3 %, 1.9 %, and 2.4 %, respectively, indicating the effectiveness of flipping even for non-zero initials. On another dataset with low z -values, the three flipping variants obtain remarkable advancements over their bases achieving 16.5 %, 24.2 %, and 17.8 % on average. Notably, flipping methods perform best except for Squirrel (with high z and low homophily). This may imply that a slight perturbation to the input features can have a greater impact than aggregation scheme modifications under semi-supervised settings.

The performance is highly related to the homophily ratio. As stated in Eq. 22, message-passing GNNs utilize the homophily property commonly observed in graphs [Lim et al., 2021, Yan et al., 2021]. In three citation graphs, GNNs outperform Multi-Layer Perceptron (MLP) due to higher homophily ratios in these graphs. However, in other datasets like Actor and three WebKB networks, Flip-MLP achieves the best accuracy among the baselines, indicating that message-passing fails to generalize well in the presence of high heterophily. The performance gain of Flip-MLP is higher than Flip-GNNs on homophilic graphs, but GNNs benefit more from flipping on heterophilic graphs. Although the APPNP method performs best on homophilic graphs, and some methods (H_2 GCN, FAGCN) outperform GCN on heterophilic networks, our flipping methods surpass these algorithms for all graph datasets.

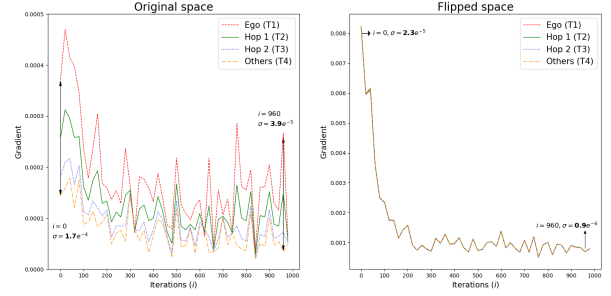


Figure 5: (RQ3) Using the Cora dataset, we plot the magnitude of the first projection matrix gradients and their standard deviation (σ) during training epochs (i)

4.3 CONVERGENCE ANALYSIS (RQ2)

One may argue that flipping could negatively impact the stability of the algorithms due to the operations in two spaces. Figure 4 illustrates the performance of vanilla GCN and GAT compared to Flip-GCN in both spaces as a function of the number of iterations, with results shown for four datasets due to limited space. The performance of GCN (blue), GAT (pink), Flip-GCN (*o*) in the original space (red), and Flip-GCN (*f*) in the flipped space (green) are depicted with different colors. The x-axis represents the training epochs, and the y-axis shows the node classification accuracy.

Through this figure, we can see that the flip-GCN achieves higher performance than plain algorithms on both spaces. In the Chameleon graph, please note that flip-GCN (*f*) surpasses the baselines after 1000 epochs. In comparison to GCN and GAT, the flip-based method demonstrates stability and fast convergence, as seen in the Chameleon and Squirrel datasets. This aligns with our analysis, as flipping reduces the variance of predictions, as described in Section 3.4. Though we admit that the performance gain of flip-GCN is dependent on the type of initial features, flip leads to the faster convergence of a model as described in the Chameleon and Squirrel dataset. In conclusion, as a data augmentation strategy, flipping leads to improved performance on datasets with multiple zero elements, while ensuring stable convergence and robustness, which is important in semi-supervised settings.

4.4 ANALYSIS OF GRADIENTS ON TWO SPACES (RQ3)

Figure 5 analyzes the gradient of the first projection matrix during the training phase with the Cora dataset. We apply different ranges of neighboring nodes and define four types: T1, T2, T3, and T4. T1 only consists of the features of the central node (Ego). T2 and T3 include the features of 1-hop and 2-hop neighbors, respectively. T4 consists of the remaining features. We prioritize the types from T1 to T4 to

Table 3: (RQ4) Node classification accuracy (%) w.r.t. the different number of training samples. The symbol (+F) means that flipping is applied on a base method

Dataset	Cora			Chameleon			Cornell		
	20	40	80	20	40	80	5	10	20
L/C									
z	0.59	0.76	0.91	1	1	1	0.62	0.72	0.84
MLP	53.2	56.9	62.1	41.2	46.3	49.1	60.1	68.8	73.3
MLP+F	61.4	65.5	70.4	43.5	49.9	51.8	70.5	86.4	95.8
GCN	79.1	82.8	83.4	49.4	53.5	55.7	39.4	50.7	53.3
GCN+F	82.7	84.5	85.5	50.4	54.1	55.9	49.4	54.9	72.8
GAT	80.1	82.4	83.0	46.9	52.4	54.1	42.1	48.9	53.3
GAT+F	83.1	84.0	84.6	48.3	52.9	54.4	51.9	59.5	64.4

avoid overlap and double-counting of features (note that all $T \in \mathcal{R}^F$ are binarized vectors).

In Figure 5, the average and standard deviation of gradients in two spaces are plotted using different colors. In the original space (left), the largest gradient is given to features from T1 (red). This is due to the property of GCN, where the gradients generally decrease w.r.t. the hop counts. Also, the features in T4 (orange) have the smallest values, suggesting that they are mostly excluded during training, with only slight updates made by weight regularization. On the other hand, in the flipped space (right), all types tend to have a similar magnitude with a small deviation (σ) since most dimensions are updated during training.

4.5 VARYING THE SIZE OF TRAINING SAMPLES (RQ4)

In this experiment, we aim to investigate the impact of labeled sample size on performance in a semi-supervised learning setting. Table 3 displays the z-value of central nodes based on the number of labeled nodes per class (L/C) for three graphs. Here, we adjust the number of training samples to analyze the effect on performance.

Firstly, we can see that GCN and GAT outperform MLP for Cora and Chameleon, while MLP surpasses two models in the Cornell dataset. It shows consistent results even when the L/C increases. Apart from this, we observe that the performance improvement from flipping decreases as the L/C increases. This is because, with more available training nodes, the initial features start to cover most dimensions (high z-value) and the plain models can effectively update the first weight matrix.

In the Chameleon graph, flipping does not have a significant impact on performance as the number of samples increases. This is because the initial features of the dataset are non-zero and have high maximum values, and as the number of labeled nodes increases, the vanilla GCN can perform well as the first hyperplane can generalize without flipping. The same trend can be seen for GAT, where the performance gap between GAT and GAT+F becomes smaller as the number of labeled nodes per class (L/C) increases. However, flipping still improves the performance of the base models in

other graphs (Cora and Cornell) significantly, which can contribute to securing robustness and generalization under semi-supervised settings.

5 RELATED WORK

Graph Neural Networks. Generally, GNNs can be divided into two categories: spectral-based and spatial-based. Spectral-based GNNs establish a mathematical foundation for graph convolution operations in the spectral domain using the Laplacian matrix [Bruna et al., 2013, Defferrard et al., 2016, Dong et al., 2021]. On the other hand, spatial-based GNNs aggregate information from local neighborhoods from a spatial perspective, leading to the development of many aggregation schemes for handling noisy connections [Velickovic et al., 2017, Pei et al., 2020, Zhu et al., 2020, Chien et al., 2020, Bo et al., 2021]. The issue of sparse initial features, however, has not received much attention in the literature.

Generalization of neural networks. In the field of neural network generalization, many approaches have been proposed [Chen et al., 2017a, Feng and Simon, 2017, Wang et al., 2021]. Several suggested the normalization of deep neural networks [Huang et al., 2020] while others applied regularization to all adjacent nodes [Yang et al., 2021] or integrated label propagation to give further information [Wang and Leskovec, 2020]. More recently, the orthogonal GCN [Guo et al., 2022] attacks the gradient vanishing problem at the initial few layers of GNNs. RawlsGCN [Kang et al., 2022] claims the unfairness of gradient update which is biased to nodes with a large degree. Though these methods show notable improvements under the semi-supervised scenario, they fail to solve the problem that is inherently occurred by a characteristic of initial features. In this paper, we solve this problem through a simple yet effective method, flipping.

6 CONCLUSION

Existing GNNs have primarily focused on optimizing the aggregation strategy while neglecting the type of initial features. In this paper, we examine the correlation between zero elements in input vectors and their impact on the first layer of neural networks. We introduce a co-training approach that involves learning the gradient flows in both the original and flipped spaces, and adaptively adjusting the parameters. Additionally, we provide a theoretical understanding that flipping reduces prediction variance while maintaining stable convergence. By incorporating flipping into three base methods, we observe an improvement in node classification accuracy, demonstrating that our approach is scalable and effective. In future work, we hope to apply flipping to other variations of GNNs to enhance their performance.

REFERENCES

- [Bo et al., 2021] Bo, D., Wang, X., Shi, C., and Shen, H. (2021). Beyond low-frequency information in graph convolutional networks. *arXiv preprint arXiv:2101.00797*.
- [Brody et al., 2021] Brody, S., Alon, U., and Yahav, E. (2021). How attentive are graph attention networks? *arXiv preprint arXiv:2105.14491*.
- [Bruna et al., 2013] Bruna, J., Zaremba, W., Szlam, A., and LeCun, Y. (2013). Spectral networks and locally connected networks on graphs. *arXiv preprint arXiv:1312.6203*.
- [Cai et al., 2021] Cai, T., Luo, S., Xu, K., He, D., Liu, T.-y., and Wang, L. (2021). Graphnorm: A principled approach to accelerating graph neural network training. In *International Conference on Machine Learning*, pages 1204–1215. PMLR.
- [Chen et al., 2017a] Chen, J., Zhu, J., and Song, L. (2017a). Stochastic training of graph convolutional networks with variance reduction. *arXiv preprint arXiv:1710.10568*.
- [Chen et al., 2020a] Chen, M., Wei, Z., Huang, Z., Ding, B., and Li, Y. (2020a). Simple and deep graph convolutional networks. In *International Conference on Machine Learning*, pages 1725–1735. PMLR.
- [Chen et al., 2020b] Chen, S., Dobriban, E., and Lee, J. H. (2020b). A group-theoretic framework for data augmentation. *The Journal of Machine Learning Research*, 21(1):9885–9955.
- [Chen et al., 2017b] Chen, Y., Li, J., Xiao, H., Jin, X., Yan, S., and Feng, J. (2017b). Dual path networks. *Advances in neural information processing systems*, 30.
- [Chien et al., 2020] Chien, E., Peng, J., Li, P., and Milenkovic, O. (2020). Adaptive universal generalized pagerank graph neural network. *arXiv preprint arXiv:2006.07988*.
- [Defferrard et al., 2016] Defferrard, M., Bresson, X., and Vandergheynst, P. (2016). Convolutional neural networks on graphs with fast localized spectral filtering. *Advances in neural information processing systems*, 29.
- [Dong et al., 2021] Dong, Y., Ding, K., Jalaian, B., Ji, S., and Li, J. (2021). Graph neural networks with adaptive frequency response filter. *arXiv preprint arXiv:2104.12840*.
- [Feng and Simon, 2017] Feng, J. and Simon, N. (2017). Sparse-input neural networks for high-dimensional non-parametric regression and classification. *arXiv preprint arXiv:1711.07592*.
- [Gilmer et al., 2017] Gilmer, J., Schoenholz, S. S., Riley, P. F., Vinyals, O., and Dahl, G. E. (2017). Neural message passing for quantum chemistry. In *International conference on machine learning*, pages 1263–1272. PMLR.
- [Guo et al., 2022] Guo, K., Zhou, K., Hu, X., Li, Y., Chang, Y., and Wang, X. (2022). Orthogonal graph neural networks. In *Proceedings of the AAAI Conference on Artificial Intelligence*, volume 36, pages 3996–4004.
- [Hamilton et al., 2017] Hamilton, W., Ying, Z., and Leskovec, J. (2017). Inductive representation learning on large graphs. *Advances in neural information processing systems*, 30.
- [Huang et al., 2020] Huang, L., Qin, J., Zhou, Y., Zhu, F., Liu, L., and Shao, L. (2020). Normalization techniques in training dnns: Methodology, analysis and application. *arXiv preprint arXiv:2009.12836*.
- [Jin et al., 2021] Jin, W., Derr, T., Wang, Y., Ma, Y., Liu, Z., and Tang, J. (2021). Node similarity preserving graph convolutional networks. In *Proceedings of the 14th ACM international conference on web search and data mining*, pages 148–156.
- [Kang et al., 2022] Kang, J., Zhu, Y., Xia, Y., Luo, J., and Tong, H. (2022). Rawlsgcn: Towards rawlsian difference principle on graph convolutional network. In *Proceedings of the ACM Web Conference 2022*, pages 1214–1225.
- [Kim and Oh, 2022] Kim, D. and Oh, A. (2022). How to find your friendly neighborhood: Graph attention design with self-supervision. *arXiv preprint arXiv:2204.04879*.
- [Kim et al., 2019] Kim, H., Rasch, M., Gokmen, T., Ando, T., Miyazoe, H., Kim, J.-J., Rozen, J., and Kim, S. (2019). Zero-shifting technique for deep neural network training on resistive cross-point arrays. *arXiv preprint arXiv:1907.10228*.
- [Kipf and Welling, 2016] Kipf, T. N. and Welling, M. (2016). Semi-supervised classification with graph convolutional networks. *arXiv preprint arXiv:1609.02907*.
- [Klicpera et al., 2018] Klicpera, J., Bojchevski, A., and Günnemann, S. (2018). Predict then propagate: Graph neural networks meet personalized pagerank. *arXiv preprint arXiv:1810.05997*.
- [Li and Yuan, 2017] Li, Y. and Yuan, Y. (2017). Convergence analysis of two-layer neural networks with relu activation. *Advances in neural information processing systems*, 30.
- [Lim et al., 2021] Lim, D., Hohne, F., Li, X., Huang, S. L., Gupta, V., Bhalerao, O., and Lim, S. N. (2021). Large scale learning on non-homophilous graphs: New benchmarks and strong simple methods. *Advances in Neural Information Processing Systems*, 34:20887–20902.

- [Lin et al., 2020] Lin, M., Ji, R., Xu, Z., Zhang, B., Wang, Y., Wu, Y., Huang, F., and Lin, C.-W. (2020). Rotated binary neural network. *Advances in neural information processing systems*, 33:7474–7485.
- [Liu et al., 2022] Liu, H., Hu, B., Wang, X., Shi, C., Zhang, Z., and Zhou, J. (2022). Confidence may cheat: Self-training on graph neural networks under distribution shift. In *Proceedings of the ACM Web Conference 2022*, pages 1248–1258.
- [Luo et al., 2021] Luo, D., Cheng, W., Yu, W., Zong, B., Ni, J., Chen, H., and Zhang, X. (2021). Learning to drop: Robust graph neural network via topological denoising. In *Proceedings of the 14th ACM International Conference on Web Search and Data Mining*, pages 779–787.
- [McPherson et al., 2001] McPherson, M., Smith-Lovin, L., and Cook, J. M. (2001). Birds of a feather: Homophily in social networks. *Annual review of sociology*, 27(1):415–444.
- [Pei et al., 2020] Pei, H., Wei, B., Chang, K. C.-C., Lei, Y., and Yang, B. (2020). Geom-gcn: Geometric graph convolutional networks. *arXiv preprint arXiv:2002.05287*.
- [Popescu et al., 2009] Popescu, M.-C., Balas, V. E., Perescu-Popescu, L., and Mastorakis, N. (2009). Multi-layer perceptron and neural networks. *WSEAS Transactions on Circuits and Systems*, 8(7):579–588.
- [Rong et al., 2019] Rong, Y., Huang, W., Xu, T., and Huang, J. (2019). Dropedge: Towards deep graph convolutional networks on node classification. *arXiv preprint arXiv:1907.10903*.
- [Rozemberczki et al., 2019] Rozemberczki, B., Davies, R., Sarkar, R., and Sutton, C. (2019). Gemsec: Graph embedding with self clustering. In *Proceedings of the 2019 IEEE/ACM international conference on advances in social networks analysis and mining*, pages 65–72.
- [Shijie et al., 2017] Shijie, J., Ping, W., Peiyi, J., and Siping, H. (2017). Research on data augmentation for image classification based on convolution neural networks. In *2017 Chinese automation congress (CAC)*, pages 4165–4170. IEEE.
- [Singla et al., 2021] Singla, V., Ge, S., Ronen, B., and Jacobs, D. (2021). Shift invariance can reduce adversarial robustness. *Advances in Neural Information Processing Systems*, 34:1858–1871.
- [Tang et al., 2009] Tang, J., Sun, J., Wang, C., and Yang, Z. (2009). Social influence analysis in large-scale networks. In *Proceedings of the 15th ACM SIGKDD international conference on Knowledge discovery and data mining*, pages 807–816.
- [Velickovic et al., 2017] Velickovic, P., Cucurull, G., Casanova, A., Romero, A., Lio, P., and Bengio, Y. (2017). Graph attention networks. *stat*, 1050:20.
- [Wang and Leskovec, 2020] Wang, H. and Leskovec, J. (2020). Unifying graph convolutional neural networks and label propagation. *arXiv preprint arXiv:2002.06755*.
- [Wang et al., 2021] Wang, X., Liu, H., Shi, C., and Yang, C. (2021). Be confident! towards trustworthy graph neural networks via confidence calibration. *Advances in Neural Information Processing Systems*, 34:23768–23779.
- [Xiao et al., 2021] Xiao, T., Chen, Z., Wang, D., and Wang, S. (2021). Learning how to propagate messages in graph neural networks. In *Proceedings of the 27th ACM SIGKDD Conference on Knowledge Discovery & Data Mining*, pages 1894–1903.
- [Xu et al., 2018] Xu, K., Hu, W., Leskovec, J., and Jegelka, S. (2018). How powerful are graph neural networks? *arXiv preprint arXiv:1810.00826*.
- [Yan et al., 2021] Yan, Y., Hashemi, M., Swersky, K., Yang, Y., and Koutra, D. (2021). Two sides of the same coin: Heterophily and oversmoothing in graph convolutional neural networks. *arXiv preprint arXiv:2102.06462*.
- [Yang et al., 2021] Yang, H., Ma, K., and Cheng, J. (2021). Rethinking graph regularization for graph neural networks. In *Proceedings of the AAAI Conference on Artificial Intelligence*, volume 35, pages 4573–4581.
- [Yang et al., 2019] Yang, L., Wu, F., Wang, Y., Gu, J., and Guo, Y. (2019). Masked graph convolutional network. In *IJCAI*, pages 4070–4077.
- [Ying et al., 2019] Ying, Z., Bourgeois, D., You, J., Zitnik, M., and Leskovec, J. (2019). Gnnexplainer: Generating explanations for graph neural networks. *Advances in neural information processing systems*, 32.
- [Zhang et al., 2017] Zhang, X., Liu, L., Xie, Y., Chen, J., Wu, L., and Pietikainen, M. (2017). Rotation invariant local binary convolution neural networks. In *Proceedings of the IEEE International Conference on Computer Vision Workshops*, pages 1210–1219.
- [Zhu et al., 2020] Zhu, J., Yan, Y., Zhao, L., Heimann, M., Akoglu, L., and Koutra, D. (2020). Beyond homophily in graph neural networks: Current limitations and effective designs. *Advances in Neural Information Processing Systems*, 33:7793–7804.
- [Zhu et al., 2021] Zhu, Y., Xu, Y., Yu, F., Liu, Q., Wu, S., and Wang, L. (2021). Graph contrastive learning with adaptive augmentation. In *Proceedings of the Web Conference 2021*, pages 2069–2080.

SUPPLEMENTARY MATERIAL

A. Input Features and Parameter Updates

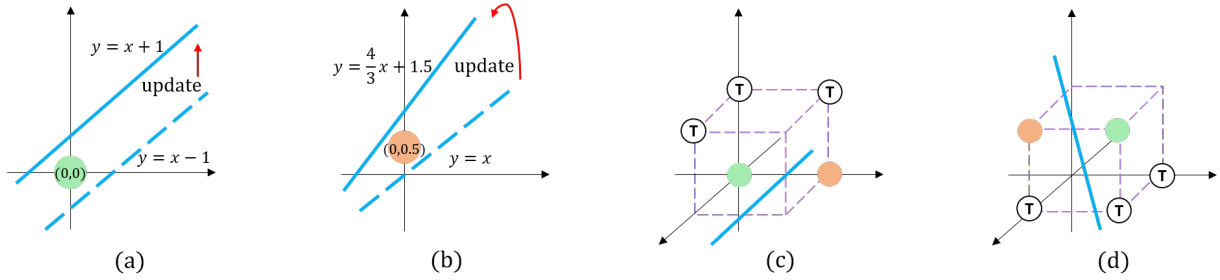


Figure 6: Analysis on gradient update and the examples of node classification. The dotted line is the line before the update, and the solid one can be derived after back-propagation. (a) All elements of input consist of zero and only the bias term is updated. (b) Non-zero value updates the hyperplane. All points in (c) and (d) share the same marginal distribution but the hyperplanes are updated differently

Figure 6a and 6b shows two examples that use 2-dimensional input data X and a single hyperplane (line). Here, we exclude the activation layer. Let us assume the true label y of this node is -1. Firstly, we define an objective function that measures the discrepancy between the predicted and true labels as,

$$\hat{y} = W^T X = \sum_{i=1}^2 W_i X_i + b,$$

$$\nabla_{W_j} \mathcal{L} = \eta(y - \hat{y}) X_j.$$

Simply, we assume the learning ratio η as 1. Thus, W can be updated as

$$\begin{pmatrix} W'_1 \\ W'_2 \end{pmatrix} = \begin{pmatrix} W_1 - X_1(1 - \hat{y}) \\ W_2 - X_2(1 - \hat{y}) \end{pmatrix},$$

and also the bias term is updated to $b' = b - (-1 - \hat{y})$.

Back into Figure 6a, let us assume the initial line is $y = x - 1$. Since the value of input features $X = (0, 0)$, the weights W are not updated. Instead, the bias becomes 1 $b' = -1 - (-1 - 1) = 1$ and successfully predicts its label as -1.

Likewise, in Figure 6b, let us consider a line and initial features as $y = x$ and $(0, 0.5)$, respectively. Then, the weights are updated to

$$\begin{pmatrix} W'_1 \\ W'_2 \end{pmatrix} = \begin{pmatrix} -1 - 0 * (1 - (0.5)) \\ 1 - 0.5 * (1 - (0.5)) \end{pmatrix} = \begin{pmatrix} -1 \\ 0.75 \end{pmatrix}.$$

and the bias becomes 0.5 $b' = 0 - (-1 - (0.5)) = 1.5$. Consequently, W becomes $y = \frac{4}{3}x + 1.5$ which also classifies this node $(0, 0.5)$ as -1. The main observation is that the updates of the hyperplane are quite sensitive to the input vectors, even though both of them make correct predictions.

In Fig. 6c and 6d, we assume two types of inputs that are symmetrical to p_1 . As can be seen in both figures, the hyperplane well separates the colored training nodes (orange and green). Nonetheless, the plane in Fig. 6c may fail to classify the test nodes T, where the z -dimensional axis has not been updated during training. On the contrary, the flipped nodes with non-zero elements can guide the parameters precisely, which helps the generalization of the hyperplane on the entire dimensions.

B. Analysis on Shifting Features

We suggest that shifting may be one of the solutions that reduce the gradient vanishing problem. Practically, adding a small value X_s to the initial feature X removes the zero elements. In Table 4 and Figure 7, we describe the node classification

Table 4: Node classification accuracy (%) on six benchmark datasets. We describe X_s with the best performance

Methods	MLP	MLP+S	X_s	GCN	GCN+S	X_s	Flip-GCN
Cora	53.2	53.5	0.01	79.1	82.7	0.2	82.7
Citeseer	53.7	54.6	0.05	67.5	70.5	0.1	72.4
Actor	27.9	27.9	0	20.4	25.9	0.9	28.6
Cornell	60.1	60.1	0	39.4	49.4	0.5	49.4
Texas	65.8	71.4	0.2	47.6	53.0	0.1	62.2
Wisconsin	73.5	73.5	0	40.5	50.2	0.1	52.3

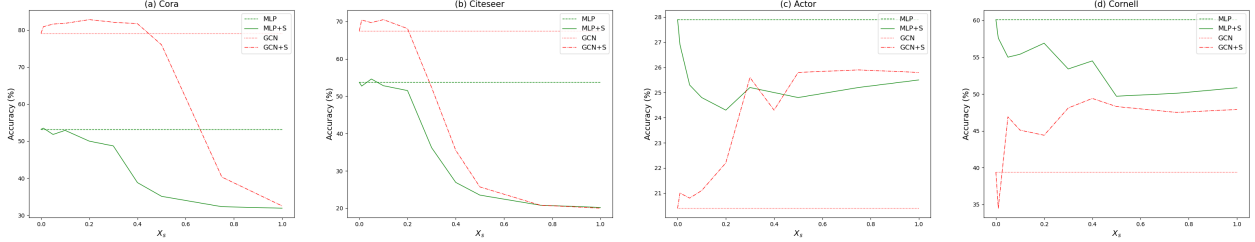


Figure 7: Variation of node classification accuracy w.r.t. the shifted value X_s on four benchmark datasets

accuracy of two baselines (MLP, GCN) using original input X , and with shifted input $X + X_s$ (MLP+S, GCN+S). The symbol (+S) means shifting is applied to the original baseline. For comparison, we also illustrate the accuracy of Flip-GCN. Here, three datasets (Pubmed, Chameleon, Squirrel) are excluded since they contain a majority of non-zero elements, which may not be appropriate for shifting and flipping. The X_s of each dataset is selected through a grid search that shows the best validation score.

In Figure 7, we can see that GCN enjoys the largest enhancements due to shifting, where its performance has improved for all datasets. Conversely, the performance of MLP generally decreases except for one dataset (Texas). We think that as the number of non-zero elements increases, a model requires more training samples. Since MLP only utilizes a central node compared to GNNs, shifting itself fails to guide the multiple parameters precisely.

C. Design Choice and Time Complexity

C.1. Design Choice

Even though plane GNN guarantees the convergence to a local optimum, the initial features might incur overfitting in the first hyperplane. Consequently, GNNs occasionally fail to learn the meaning of entire dimensions when bag-of-words are adopted as features. We acknowledge that overfitting is a complex problem and many schemes including cross-validation, dropout, regularization have been proposed to alleviate this issue. Generally, GNNs employ cross-validation, where the early stopping is used based on the validation score. We also exploit dropout after applying activation function. As described in Eq. 6, shifting might be one solution but it raises a difficult regularization issue. Therefore, we devise flipping initial features along with hyperplane, which can preserve the scale of the outputs before and after transposition. Even though our method depends on the type of input data, it is undeniable that flip achieves significant improvements through a simple modification under this condition.

C.2. Computational Complexity

To analyze the computational complexity, we divide our model into two parts. The proposed scheme consists of a vanilla GCN [Kipf and Welling, 2016] and a flipped GCN. The computational cost of vanilla GCN is known to be $\mathcal{O}(|\mathcal{E}|P_{GCN})$, where P_{GCN} is the number of learnable weights. More specifically, P_{GCN} can be decomposed [Zhu et al., 2020] into $\mathcal{O}(nz(X)F' + F'C)$, where $nz(X)$ is the number of non-zero elements in input X and F' is the dimension after projection. $F'C$ is the parameter of the second convolution layer. Also, $\mathcal{O}|\mathcal{E}| \approx \mathcal{O}|\mathcal{E}|d_{max}$ and d_{max} is the maximum degree. Similar to the vanilla GCN, the complexity of the flipped GCN can be defined as $\mathcal{O}(|\mathcal{E}|P'_{GCN})$. In detail,

$P'_{GCN} = \mathcal{O}(nz(X_f)F' + F'C)$ where $nz(X_f)$ is the number of non-zero elements in flipped features. Summarizing the above two equations, the complexity of our model is $\mathcal{O}(|\mathcal{E}|(P_{GCN} + P'_{GCN}))$, which is proportional to the number of edges ($|\mathcal{E}|$) and the size of learnable matrices ($P_{GCN} + P'_{GCN}$).

D. More Details of Baselines and Implementation

D.1. Baselines

- **MLP** [Popescu et al., 2009] adopts a feed-forward neural network without message-passing.
- **GCN** [Kipf and Welling, 2016] suggests the first-order approximation of Chebyshev polynomials [Defferrard et al., 2016] to preserve low frequency signals between neighbors.
- **DropEdge** [Rong et al., 2019] randomly deletes edges based on a given probability in order to alleviate over-fitting.
- **Ortho-GCN** [Guo et al., 2022] maintains the orthogonality of feature transformation matrices through three constraints.
- **GIN** [Xu et al., 2018] adopts an injective mapping function to enhance the discriminative power of GCN and ensures isomorphism.
- **GAT** [Velickovic et al., 2017] employs node features to assign different weights for each edge without graph structural property.
- **GATv2** [Brody et al., 2021] improves GAT to generate a more dynamic graph attention that is more expressive.
- **APPNP** [Klicpera et al., 2018] combines personalized PageRank with GCN to improve accuracy while reducing the computational cost.
- **GCNII** [Chen et al., 2020a] further utilizes the weighted identity mapping function to redeem the deficiency of APPNP.
- **H₂GCN** [Zhu et al., 2020] separates ego from neighbors and applies hop-based aggregation for heterophilic networks.
- **P-reg** [Yang et al., 2021] improves the traditional graph Laplacian to provide extra information that GNNs might not capture.
- **FAGCN** [Bo et al., 2021] adaptively controls the propagation of low and high-frequency signals during message passing.

D.2. Implementation

We implemented the baselines and our method using *PyTorch Geometric*¹. In detail, two layers of GNNs are used for all baselines except for APPNP and GCNII. The hidden dimension is set as 64 and we adopted the ReLU with dropout as an activation function. The log Softmax is applied for classification. A learning ratio of ($1e^{-3}$) and the Adam optimizer with a weight decay ($5e^{-4}$) are used for training. We randomly chose 20 nodes per class as training samples except for the WebKB dataset whose size is smaller than the others. The remaining nodes are randomly and equally divided into validation and testing nodes. The test accuracy is measured at each iteration, and we selected one that achieves the best validation score. Our source code is also available at anonymous *github*². In addition to Flip-GCN, we describe the details of Flip-MLP and Flip-GAT below.

E. Details of Flip-MLP and Flip-GAT

E.1. Flip-MLP is a simple modification of Flip-GCN, where the message-passing (A) is removed as below:

In an original space,

$$\begin{aligned} H_o^{(2)} &= \sigma(X_o W_o^{(1)}), \quad (l = 1) \\ H_o^{(l+1)} &= \sigma(\bar{H}_o^{(l+1)}), \quad \bar{H}_o^{(l+1)} = H_o^{(l)} W_o^{(l)}, \quad (l \geq 2) \end{aligned} \tag{23}$$

¹<https://pytorch-geometric.readthedocs.io/en/latest/modules/nn.html>

²<https://anonymous.4open.science/r/Flip-GNN-EAA5>

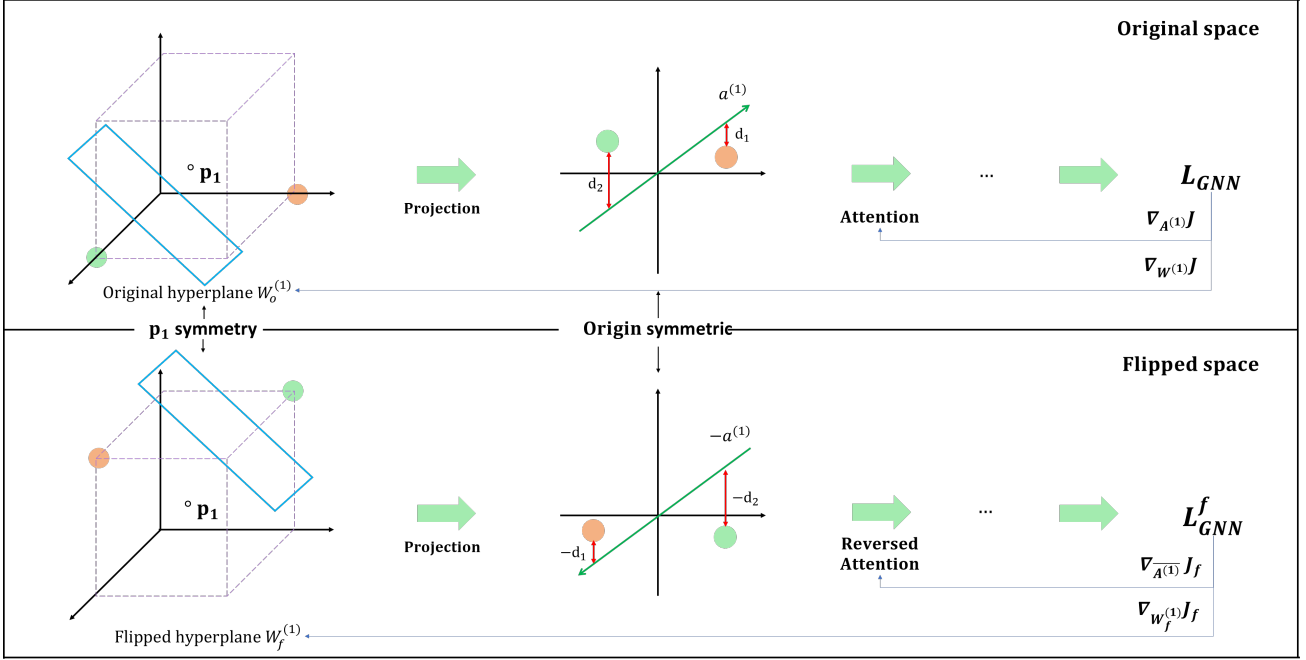


Figure 8: The overview of the first layer in Flip-GAT. Compared to Flip-GCN, Flip-GAT contains an additional attention layer $a^{(1)}$ that has to be considered during back-propagation

In the flipped space,

$$\begin{aligned}
 H_f^{(2)} &= -\sigma(X_f W_f^{(1)}), \quad (l = 1) \\
 H_f^{(l+1)} &= \sigma(\bar{H}_f^{(l+1)}), \quad \bar{H}_f^{(l+1)} = H_f^{(l)} W_f^{(l)}, \quad (l \geq 2)
 \end{aligned} \tag{24}$$

E.2. Flip-GAT is illustrated in Figure 8. Since plane GAT [Velickovic et al., 2017] employs an attention layer, we should consider this in both spaces. Firstly, we discuss the forward propagation in an original space as below:

$$\begin{aligned}
 A_{ij}^{(l)} &= \frac{\exp(\sigma(a^{(l)}[h_i^{(l)} || h_j^{(l)}]))}{\sum_{k \in N_i} \exp(\sigma(a^{(l)}[h_i^{(l)} || h_k^{(l)}]))}, \quad (l \geq 1) \\
 H_o^{(l+1)} &= \sigma(\bar{H}_o^{(l+1)}), \quad \bar{H}_o^{(l+1)} = A^{(l)} H_o^{(l)} W_o^{(l)}
 \end{aligned}$$

During back-propagation, the gradients of W , a multi-head projection matrix, are defined as follows:

$$\nabla_{W_o^{(l)}} J_o = (A^{(l)} H_o^{(l)})^T \nabla_{\bar{H}_o^{(l+1)}} J_o, \quad (l \geq 1).$$

Also, we can retrieve the gradients of the attention layer as below:

$$\nabla_{A_o^{(l)}} J = (H_o^{(l)} W_o^{(l)})^T \nabla_{\bar{H}_o^{(l+1)}} J_o, \quad (l \geq 1).$$

In a flipped space, the forward propagation is quite similar to Flip-GCN but we should multiply the negative constant (-1) on the first attention layer. As described in the middle of Figure 8, the attention values d_1, d_2 are origin symmetry. Thus, the forward propagation is defined as follows:

$$\begin{aligned}
 \bar{A}_{ij}^{(1)} &= \frac{\exp(\sigma(-a^{(1)}[h_i^{(1)} || h_j^{(1)}]))}{\sum_{k \in N_i} \exp(\sigma(-a^{(1)}[h_i^{(1)} || h_k^{(1)}]))} \\
 H_f^{(2)} &= -\sigma(\bar{A}^{(1)} X_f W_f^{(1)}), \quad (l = 1), \\
 H_f^{(l+1)} &= \sigma(\bar{H}_f^{(l+1)}), \quad \bar{H}_f^{(l+1)} = A^{(l)} H_f^{(l)} W_f^{(l)}, \quad (l \geq 2)
 \end{aligned}$$

Likewise, we obtain the gradients of W as,

$$\begin{aligned}\nabla_{W_f^{(1)}} J_f &= (\bar{A}^{(1)} X_f)^T \nabla_{\bar{H}_f^{(2)}} J_f, \quad \bar{H}_f^{(2)} = \bar{A}^{(1)} X_f W_f^{(1)}, \quad (l = 1) \\ \nabla_{W_f^{(l)}} J_f &= (A^{(l)} H_f^{(l)})^T \nabla_{\bar{H}_f^{(l+1)}} J_f, \quad (l \geq 2).\end{aligned}$$

Similarly, the attention vectors are updated as below:

$$\begin{aligned}\nabla_{\bar{A}^{(1)}} J_f &= -(H_f^{(1)} W_f^{(1)})^T \nabla_{\bar{H}_f^{(2)}} J_f, \quad (l = 1) \\ \nabla_{A^{(l)}} J_f &= (H_f^{(l)} W_f^{(l)})^T \nabla_{\bar{H}_f^{(l+1)}} J_f, \quad (l \geq 2).\end{aligned}$$